

## RESEARCH ARTICLE

10.1002/2013JD020199

## Key Points:

- First analysis of quasi 2 day wave in NH summer with data assimilation system
- Quasi 2 day wave sources found near core of mesospheric easterly jet
- Baroclinic instability triggers quasi 2 day wave

## Correspondence to:

J. P. McCormack,  
john.mccormack@nrl.navy.mil

## Citation:

McCormack, J. P., L. Coy, and W. Singer (2014), Intraseasonal and interannual variability of the quasi 2 day wave in the Northern Hemisphere summer mesosphere, *J. Geophys. Res. Atmos.*, 119, 2928–2946, doi:10.1002/2013JD020199.

Received 15 MAY 2013

Accepted 24 FEB 2014

Accepted article online 26 FEB 2014

Published online 20 MAR 2014

## Intraseasonal and interannual variability of the quasi 2 day wave in the Northern Hemisphere summer mesosphere

J. P. McCormack<sup>1</sup>, L. Coy<sup>2,3</sup>, and W. Singer<sup>4</sup>

<sup>1</sup>Space Science Division, Naval Research Laboratory, Washington, District of Columbia, USA, <sup>2</sup>Global Modeling and Assimilation Office, NASA Goddard Space Flight Center, Greenbelt Maryland, USA, <sup>3</sup>Science Systems and Applications Incorporated, Lanham Maryland, USA, <sup>4</sup>Leibniz-Institute of Atmospheric Physics, University of Rostock, Kühlungsborn, Germany

**Abstract** This study uses global synoptic meteorological fields from a high-altitude data assimilation system to investigate the quasi 2 day wave (Q2DW) and migrating diurnal tide during the Northern Hemisphere (NH) summers of 2007–2009. By applying a two-dimensional fast Fourier transform to meridional wind and temperature fields, we identify Q2DW source regions and diagnose propagation of Q2DW activity into the upper mesosphere and lower thermosphere. We find that the Q2DW in NH summer is composed primarily of westward propagating zonal wave number 3 and wave number 4 components that originate within baroclinically unstable regions along the equatorward flank of the summer midlatitude easterly jet. The amplitude of the wave number 3 Q2DW tends to peak in July while the amplitude of the wave number 4 Q2DW tends to peak in late June and again in early August. The seasonal mean Q2DW amplitudes are largest in 2009, when the amplitude of the migrating diurnal tide in the upper mesosphere near 30°N was relatively weak. However, there is no evidence of rapid amplification of the Q2DW via nonlinear interaction with the diurnal tide. Instead, variations of Q2DW amplitudes during NH summer appear to be linked to variations in the strength and location of the mesospheric easterly jet from one summer to the next, with a stronger jet producing larger Q2DW amplitudes. Linear instability model calculations based on the assimilated wind fields indicate that the fastest-growing modes are zonal wave numbers 3 and 4 with periods near 2 days that originate in the vicinity of the easterly jet.

## 1. Introduction

Wind and temperature observations in the mesosphere/lower thermosphere (MLT) over the last several decades show that one of the largest recurring features in MLT dynamics is a westward propagating zonal wave number 3 disturbance with a period near 48 h that is commonly referred to as the quasi 2 day wave or Q2DW [e.g., Muller and Nelson, 1978; Harris, 1994; Lima et al., 2004; Pancheva, 2006; Hecht et al., 2010; Suresh Babu et al., 2011]. Satellite-based measurements of temperature and long-lived constituents [e.g., Wu et al., 1996; Limpasuvan and Wu, 2003; Garcia et al., 2005; Tunbridge et al., 2011], in combination with satellite-based wind observations [Wu et al., 1993; Lieberman, 1999; Limpasuvan and Wu, 2009; Gu et al., 2013], have shown that Q2DW amplitudes peak in the extratropical MLT during both Southern Hemisphere (SH) and Northern Hemisphere (NH) summer shortly after solstice. As an example, Figure 1 plots temperature and meridional wind anomalies at 40°N and 0.02 hPa (~ 75 km) during July 2009 showing longitude-time behavior consistent with a westward propagating Q2DW.

The Q2DW originates primarily from baroclinically unstable regions near the summertime mesospheric easterly jet. Current theory indicates that these regions produce fast-growing instabilities that can project onto the zonal wave number 3 global Rossby-gravity mode [Salby, 1981; Plumb, 1983; Pfister, 1985; Lieberman, 1999; Rojas and Norton, 2007]. One key aspect of the Q2DW that is not yet well understood is the cause of its intermittency, i.e., it is often observed in “bursts” throughout the summer season (see, e.g., 1–10 July and 20–25 July in Figure 1). As a result, the observed Q2DW can exhibit a high degree of both intraseasonal and interannual variability that has been extensively documented in both ground-based and satellite-based data sets [e.g., Wu et al., 1996; Limpasuvan and Wu, 2003; Garcia et al., 2005; Tunbridge et al., 2011; Offermann et al., 2011]. Modeling studies suggest that this variability can have a wide-ranging effect on, e.g., summer polar mesopause temperatures [Pendlebury, 2012], thermospheric neutral winds [Chang et al., 2011], and

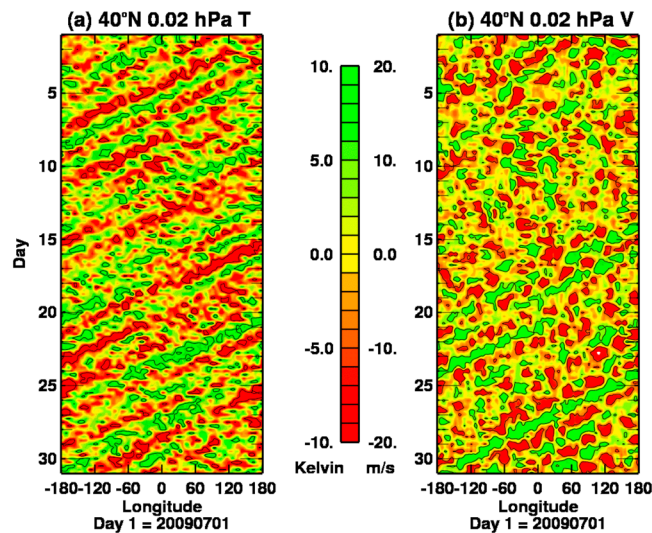


**Figure 1.** Hovmöller plot of NOGAPS-ALPHA (a) temperature and (b) meridional wind anomalies at 40°N and 0.02 hPa for July 2009. Contours are drawn at  $\pm 5$  K and  $\pm 10$  m s<sup>-1</sup>.

wave drag can trigger Q2DW activity by decelerating the summertime mesospheric easterly jet. *Salby and Callaghan* [2008] showed that the presence of the migrating diurnal solar tide in a primitive equation model can increase the damping of the Q2DW and thus limit its growth under solstice conditions through nonlinear wave-wave interactions. Nonlinear interactions between the Q2DW and the migrating diurnal tide can also cause a rapid growth in Q2DW amplitude and a contemporaneous (albeit smaller) reduction in the diurnal tidal amplitude. This process was first noted in the observational study by *Teitelbaum and Vial* [1991], and later described in several modeling studies [*Norton and Thuburn*, 1999; *Palo et al.*, 1999; *Salby and Callaghan*, 2008; *Chang et al.*, 2011]. Key factors determining whether or not this rapid amplification of the Q2DW will occur are a strong easterly jet in the summer upper mesosphere and phase locking of the Q2DW with the diurnal cycle (i.e., a 48 h period) [*Walterscheid and Vincent*, 1996]. These conditions, and subsequent Q2DW-tide interactions, have been observed in the SH summer MLT [*Hecht et al.*, 2010; *McCormack et al.*, 2010], but it is not clear whether or not such processes also contribute to variability in the Q2DW during NH summer.

Here we examine the roles of both baroclinic instability mechanisms and possible Q2DW-tidal interactions in controlling Q2DW intermittency in the NH summer extratropical MLT. Doing so requires a data set of global winds and temperatures extending throughout the MLT region with sufficient temporal resolution to separate the Q2DW and tidal signatures. Presently, such information cannot be obtained from a single set of observations, but can instead be obtained by combining multiple sets of MLT observations using a high-altitude data assimilation system (HDAS). This study examines Q2DW and tidal variability using 6-hourly synoptic meteorological analyses of winds and temperature from the surface to 90 km altitude over the June–August periods of 2007–2009 produced by the Navy Operational Global Atmospheric Prediction System with Advanced Level Physics-High Altitude (NOGAPS-ALPHA). The NOGAPS-ALPHA HDAS has been used previously to describe Q2DW variability in the SH extratropics during January [*McCormack et al.*, 2009], and to provide evidence of nonlinear Q2DW-tidal interactions in the extratropical SH summer MLT region [*McCormack et al.*, 2010]. This is the first study using HDAS fields to examine the behavior of the Q2DW and tides in the NH summer.

Although the amplitude of the Q2DW in the NH is smaller than its SH counterpart, it has a more complex spatial structure consisting of zonal wave numbers 2–4 whose relative amplitudes vary over the course of the season [*Tunbridge et al.*, 2011]. We employ space-time spectral analysis of the NOGAPS-ALPHA wind and temperature fields to discriminate among the different spatiotemporal components of the Q2DW and the diurnal tide, which is not possible using ground-based data sets or asynoptic satellite records alone, given their limitations in spatial and temporal coverage. This information is used to characterize the intraseasonal and interannual variability in the NH Q2DW in relation to the migrating diurnal tide. NOGAPS-ALPHA winds

ionospheric electron content [*Yue et al.*, 2012a]. Investigating the origins of Q2DW variability can therefore improve our overall understanding of MLT dynamics.

Conditions for baroclinic instability are extremely sensitive to gradients in background zonal wind and temperature, which in the MLT arise through complex interactions involving gravity wave drag and solar tides. *Norton and Thuburn* [1999] used a global circulation model (GCM) to demonstrate that the effect of gravity wave drag maintains the meridional and vertical gradients in the summertime MLT zonal wind distribution that are necessary for the growth of baroclinically unstable local modes. More recently, *Ern et al.* [2013] found observational evidence that enhanced gravity

are also used as input for a linear instability model to diagnose the origin and growth of the Q2DW throughout the NH summer via baroclinic instability. The results of this investigation indicate that the strength and location of the midlatitude mesospheric easterly jet core is the main factor controlling the behavior of the Q2DW during NH summer.

The NOGAPS-ALPHA HDAS system and data analysis techniques are described in section 2. Section 3 presents the intraseasonal and interannual variability in the Q2DW and diurnal migrating tide during NH summer of 2007–2009. Section 4 discusses the origin and propagation of the Q2DW using diagnostic wave activity calculations. Section 5 presents results from a linear instability model that uses NOGAPS-ALPHA assimilated winds to examine how the Q2DW arises from baroclinically unstable regions near the summer easterly jet. Section 6 contains a summary of these results and discusses future research directions.

## 2. Data and Methodology

The NOGAPS-ALPHA HDAS assimilates operational meteorological observations in the troposphere and lower stratosphere in combination with research satellite observations of middle atmospheric temperature, ozone, and water vapor to provide a comprehensive analysis of atmospheric state variables from the surface to ~90 km. In this section, we first present a brief overview of the HDAS system. For a complete description of the production version of NOGAPS-ALPHA, see *Eckermann et al.* [2009a]. We then discuss the methods used to analyze the behavior of the Q2DW and diurnal migrating tide in the NH summer MLT.

### 2.1. NOGAPS-ALPHA Description

NOGAPS-ALPHA is built upon the framework of the NOGAPS numerical weather prediction and analysis system that originally extended from the surface to 1 hPa (~50 km). It consists of two main components: a global spectral forecast model [*Hogan and Rosmond*, 1991], and a three-dimensional variational (3DVAR) data assimilation algorithm [*Daley and Barker*, 2001]. To expand this system's meteorological analysis capability through the middle atmosphere, the vertical domain of the NOGAPS-ALPHA forecast model was raised to ~100 km [*Hoppel et al.*, 2008], and a 68-level (L68) hybrid  $\sigma - p$  vertical coordinate was introduced [*Eckermann*, 2009b], giving ~2 km spacing of levels throughout the stratosphere and mesosphere. In the present study, the forecast model component of NOGAPS-ALPHA uses a T79 horizontal wave number truncation to give an effective horizontal grid spacing of 1.5° in longitude and latitude on a quadratic Gaussian grid. Extending NOGAPS-ALPHA into the middle atmosphere required the addition of several new physics packages, as described in *Eckermann et al.* [2009a]. These include improved shortwave heating and long-wave cooling rates [*Chou et al.*, 2001; *Chou and Suarez*, 2002], updated parameterizations of subgrid scale orographic [*Palmer et al.*, 1986] and nonorographic gravity wave drag [*Eckermann*, 2011], and linearized photochemical parameterizations for middle atmospheric ozone and water vapor [*McCormack et al.*, 2006; *McCormack et al.*, 2009], which are both prognostic model variables in NOGAPS-ALPHA.

The data assimilation component of NOGAPS-ALPHA is based on the NRL Atmospheric Variational Data Assimilation System [*Daley and Barker*, 2001], a 3DVAR system with a 6 h update cycle that assimilates both conventional ground-based observations (e.g., wind, pressure, and temperature from station reports and radiosondes) and operational satellite-based observations (e.g., microwave radiances, surface winds, and precipitable water). In addition, NOGAPS-ALPHA assimilates Aura MLS Version 2.2 temperature, O<sub>3</sub>, and H<sub>2</sub>O profile measurements [*Hoppel et al.*, 2008]. The Aura satellite completes ~13 orbits per day with coverage between 82°S and 82°N latitude. NOGAPS-ALPHA also assimilates Version 1.07 temperature profile measurements from the Thermosphere, Ionosphere, Mesosphere Energetics and Dynamics (TIMED) Sounding of the Atmosphere using Broadband Radiometry (SABER) instrument, which is a side-viewing instrument whose latitude coverage alternates every 2 months to view high latitudes in both hemispheres. During NH summer, in mid-July, SABER switches from its north viewing mode (latitude range of 83°N to 52°S) to south viewing mode (52°N to 83°S). This change in coverage is not seen to affect the assimilated Q2DW in the NOGAPS-ALPHA analyses, which is generally largest equatorward of 50°N.

The bulk of the information on the Q2DW and tides in the NOGAPS-ALPHA analyses comes from MLS and SABER temperature profiles that are assimilated between the 32 and 0.002 hPa pressure levels. The vertical resolution of the SABER temperature retrieval remains ~2 km throughout the stratosphere and mesosphere while the resolution of the MLS temperature retrieval degrades from ~3 km in the stratosphere to ~13 km near the 0.01 hPa level. Global mean systematic biases of 2–3 K between the MLS and SABER temperatures

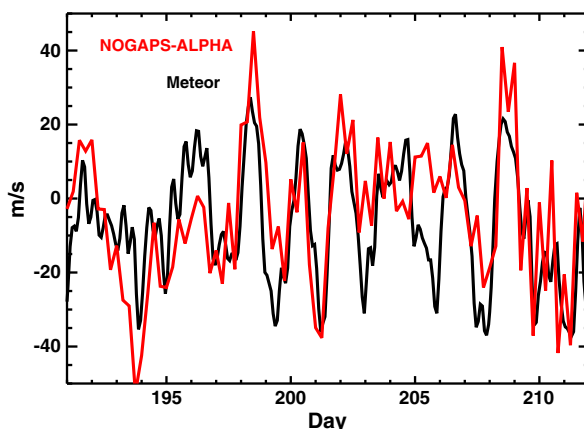


**Figure 2.** Time series of meridional winds from meteor radar observations over Kühlungsborn (54°N, 12°E) at 88 km (black curve) and from coincident NOGAPS-ALPHA analyses at 0.0036 hPa (red curve) during July–August 2007.

formulation of the gradient wind approximation in the off-diagonal elements of the observation error covariance matrix to produce balanced wind and temperature increments. These increments are integrated forward in time by the forecast model component, and the resulting middle atmospheric wind fields are further constrained by the physical parameterizations in the model (e.g., gravity wave drag, diffusion, etc.). As previous studies have shown [McCormack *et al.*, 2009, 2010] the resulting 6-hourly global wind and temperature fields have the spatial and temporal resolutions necessary to discriminate between the Q2DW and diurnal tide in the SH summer MLT; the present study extends these investigations to the NH summer.

A critical test of any assimilation system is verification with independent observations. For middle atmospheric winds and temperatures, these types of observations consist mainly of ground-based radar and lidar measurements over a relatively small number of locations. Eckermann *et al.* [2009a] and Stevens *et al.* [2010] showed that diurnal and semidiurnal variations in the NOGAPS-ALPHA MLT wind and temperature fields agree well with independent ground-based observations at high northern latitudes during the 2007 summer season. McCormack *et al.* [2010] also showed good agreement between the Q2DW in NOGAPS-ALPHA MLT winds and medium-frequency radar winds over Adelaide during January 2006 and January 2008. Furthermore, NOGAPS-ALPHA winds compared well with Tromsø meteor radar winds at 70°N during January 2009 [Coy *et al.*, 2011].

To demonstrate that NOGAPS-ALPHA MLT winds used in the present study can capture the day-to-day variability in the Q2DW seen in ground-based data sets during NH summer, Figure 2 compares meridional winds at 88 km altitude from meteor radar observations [Singer *et al.*, 2003] over Kühlungsborn (54°N, 12°E) with corresponding NOGAPS-ALPHA winds at 0.0036 hPa during July and August 2007. To facilitate the comparison, a five-point smoothing was applied to the hourly meteor wind values in order to reduce high-frequency variability. As Figure 2 shows, there is good overall agreement between the NOGAPS-ALPHA analyzed winds and the meteor radar winds at this location. Specifically, both data sets exhibit 2 day periodicities during days 195–203 with similar amplitude and phase. This agreement is notable given the fact that no wind information is directly assimilated by NOGAPS-ALPHA, as discussed in section 2. There are also times during July–August 2007 when significant differences occur between the NOGAPS-ALPHA and meteor radar winds, e.g., on days 205–206, which may be due to gravity wave activity at small scales which cannot be resolved by the assimilation system. Although additional comparisons are desirable to fully verify the NOGAPS-ALPHA analyses, results to date clearly demonstrate that the 6-hourly analyzed winds can capture key features of the Q2DW.

## 2.2. Space-Time Spectral Analysis

To describe the characteristics of the Q2DW and diurnal migrating tide, we use a two-dimensional fast Fourier transform (2DFFT) approach following Hayashi [1971], where NOGAPS-ALPHA wind and

have been removed prior to assimilation to avoid introducing spurious spatial variability into the temperature analyses, as described in the work of Hoppel *et al.* [2008]. To obtain accurate heating and cooling rates in the middle atmosphere, NOGAPS-ALPHA also assimilates daily MLS H<sub>2</sub>O and O<sub>3</sub> profiles between 220–0.002 hPa and 215–0.02 hPa, respectively [Eckermann *et al.*, 2009a].

To investigate the Q2DW in the NH MLT, the present study analyzes global synoptic zonal and meridional wind fields produced by the NOGAPS-ALPHA HDAS. NOGAPS-ALPHA does not directly assimilate middle atmospheric wind measurements; instead, it uses a

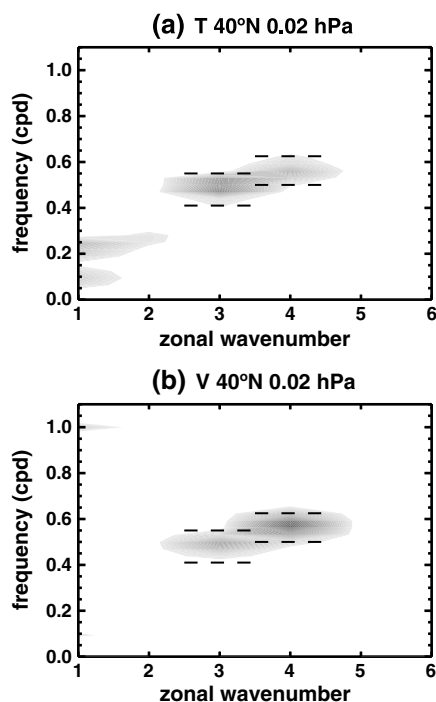


**Figure 3.** Normalized power spectra obtained from the NOGAPS-ALPHA (a) temperature and (b) meridional wind anomalies for July 2009 at 40°N and 0.02 hPa plotted in Figure 1. Positive frequencies denote westward propagation. Dashed lines denote frequency ranges of digital filters used to isolate zonal wave 3 and 4 components of the quasi 2 day wave.

wave 3 consistently peaks in the frequency range 0.4–0.53 cpd, while power at zonal wave 4 consistently peaks between 0.5 and 0.625 cpd.

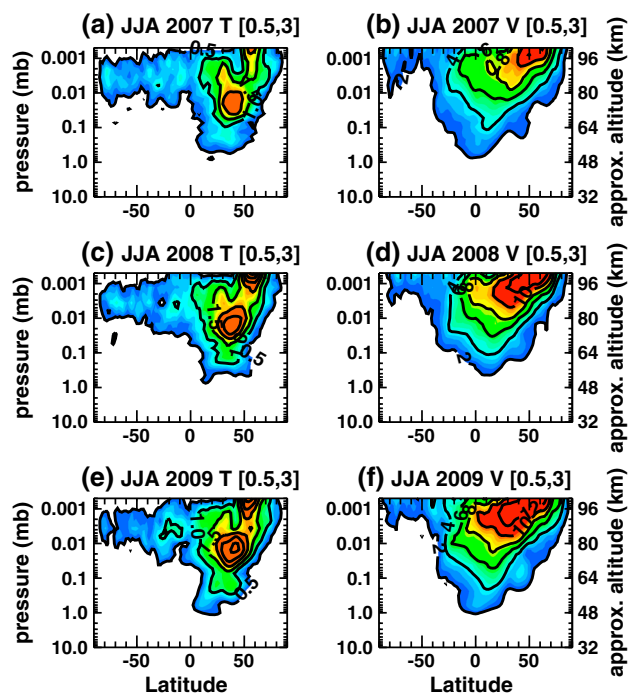
This combination of waves 3 and 4 at periods near 2 days in Figure 3 agrees with the study of MLS temperatures by *Tunbridge et al.* [2011], who found the Q2DW during July 2009 to consist primarily of westward zonal wave numbers 3 and 4. In this particular case, we do not find a westward wave 2 component in the power spectra plotted in Figure 3 at 0.02 hPa and 40°N. However, our analysis does find a relatively weak wave 2 component in both wind and temperature at altitudes above 80 km, which is discussed further in section 3.1.

Figure 3b also indicates variance in the meridional wind field at wave 1 centered on 1 cpd associated with the migrating diurnal tide. A corresponding [1,1] feature is not seen in the temperature power spectra (Figure 3a) for this particular location. This is due to the latitude structure of the temperature tide in the upper mesosphere, which peaks near the equator and falls off more rapidly with latitude than the meridional wind tide. (The altitude and latitude structure of the tidal response in temperature and meridional wind derived from the NOGAPS-ALPHA analyses is discussed in more detail in section 3.) It should be noted that although spectral analysis of the 6-hourly NOGAPS-ALPHA output can resolve frequencies down to 2 cpd, the 3DVAR system's  $\pm 3$  h assimilation window may not be able to fully capture this high-frequency variability associated with, e.g., the semidiurnal tide. Therefore, this study focuses on possible interactions between the Q2DW and diurnal tide.

To study the behavior of the Q2DW and diurnal tide throughout the NH summer season, 6-hourly longitude/time fields of the individual Q2DW and tide components in the wind and temperature fields are reconstructed by applying appropriate band-pass filters to the inverse 2DFFT. Based on the analysis of the 2DFFT power spectra described above, pass bands from 0.4–0.53 cpd to 0.5–0.625 cpd are used to isolate the westward propagating zonal wave 3 and 4 components of the Q2DW, respectively. A pass band at zonal

temperature fields at a given latitude and pressure level are expanded as Fourier series in longitude and time. Following the procedure described in *McCormack et al.* [2009], daily zonal means are subtracted from each 6-hourly longitude-time field and then a cosine taper is applied to the first and last 10% of each record in time. The resulting space-time power spectrum describes the amount of variance at each frequency and zonal wave number. The 2DFFT is applied over a 32 day interval to derive results for an individual month. It is also applied over a 75 day interval to obtain results over the summer period from early June to early August.

Figure 3 plots the resulting normalized power spectra derived for a 32 day period (128 points) of 6-hourly NOGAPS-ALPHA temperature and meridional wind fields from 30 June to 31 July 2009 at 0.02 hPa ( $\sim 75$  km) and 40°N (see Figure 1). The 2DFFT method can identify both westward and eastward propagating features that are associated, by convention, with positive and negative frequency values, respectively. At this particular level, only westward features are found and so only positive frequencies are plotted. The results of the 2DFFT in Figure 3 show that most of the variance in the NOGAPS-ALPHA temperature and meridional wind fields at this location is found in westward propagating zonal wave numbers 3 and 4 with frequencies between 0.45 and 0.60 cpd. By examining 2DFFT spectra from all NOGAPS-ALPHA temperature and wind fields over the NH from 1 to 0.002 hPa during July of 2007–2009, we find that power at zonal



**Figure 4.** Root-mean-square amplitudes of the [0.5,3] Q2DW component in temperature and meridional wind averaged over June–July–August (JJA) of (a, b) 2007, (c, d) 2008, and (e, f) 2009. Contour intervals are 0.5 K and  $2 \text{ m s}^{-1}$ .

NOGAPS-ALPHA temperature and meridional wind fields. This section also discusses both the interannual and intraseasonal variability of these features during June–August of 2007–2009.

### 3.1. Interannual Variability of the Q2DW and Diurnal Tide

Figure 4 plots mean values of the RMS amplitude for the westward propagating zonal wave number 3 component of the Q2DW in both temperature and meridional wind (referred to in terms of its primary frequency and wave number as [0.5,3]) for the June–July–August (JJA) period of 2007–2009. In all three years, the spatial structure of the temperature Q2DW between 70 and 90 km is generally consistent with earlier observations of the NH summer [e.g., Tunbridge *et al.*, 2011, Figure 7]. Specifically, we find that the feature exhibits deep vertical extent throughout the mesosphere between  $20^{\circ}\text{N}$  and  $55^{\circ}\text{N}$  with a maximum in temperature near  $40^{\circ}\text{N}$  and 0.02 hPa ( $\sim 75 \text{ km}$ ). Figure 4 also shows that the peak JJA mean temperature amplitudes in this region vary from year to year, reaching 2.2 K in 2007, 2.7 K in 2008, and 3.0 K in 2009. An analysis of the Q2DW by Gu *et al.* [2013] also found similar interannual variations, i.e., higher Q2DW amplitudes during NH summer 2009 compared to 2007 and 2008.

Another maximum in [0.5,3] temperature amplitude is noted in all three years between  $50^{\circ}\text{N}$  and  $60^{\circ}\text{N}$  above 0.002 hPa ( $\sim 90 \text{ km}$ ), reaching 2.0 K, 3.3 K, and 3.1 K in 2007, 2008, and 2009 respectively (Figures 4a, 4c, and 4e). While this feature appears to be related to the maximum in the [0.5,3] meridional wind component near 95 km (Figures 4b, 4d, and 4f), it should be regarded with some caution as it lies above the top pressure level of 0.002 hPa where MLS and SABER temperature observations are assimilated. For the purposes of this study, we limit discussion of the Q2DW to the altitude region below the 0.002 hPa level ( $\sim 90 \text{ km}$ ), where NOGAPS-ALPHA fields are constrained by observations.

The interannual variability in JJA mean meridional wind [0.5,3] amplitudes shown in Figure 4 matches that of the JJA mean temperature amplitudes. For the 3 years analyzed, the Q2DW in meridional wind is strongest in 2009 and weakest in 2007. The spatial structure of the meridional wind [0.5,3] component is consistent from year to year, exhibiting a poleward tilt with increasing height and a maximum at 90 km between  $40^{\circ}\text{N}$  and  $50^{\circ}\text{N}$ . These features are in good qualitative agreement with model simulations of the [0.5,3] feature in meridional wind [Norton and Thuburn, 1999; Palo *et al.*, 1999; Salby and Callaghan, 2000; Chang *et al.*, 2011], lending confidence in the fidelity of the NOGAPS-ALPHA meridional wind analyses.

wave number 1 from 0.9 to 1.1 cpd is used for the diurnal tide. The root-mean-square (RMS) amplitudes of the zonal wave number 1, 3, and 4 components are then calculated from the filtered fields at each latitude and pressure for every time step. Eddy heat and momentum fluxes are also calculated from these filtered fields, and are then used to formulate Eliassen–Palm (EP) flux diagnostics of wave activity associated with the Q2DW. This technique has been applied previously to NOGAPS-ALPHA fields to investigate the evolution of the Q2DW and diurnal tide in the SH summer mesosphere [McCormack *et al.*, 2009, 2010]. In the present study, we extend this analysis to focus on the NH summers of 2007–2009.

## 3. 2DFFT Results

This section presents detailed information on the latitude and altitude structure of the Q2DW and migrating diurnal tide during NH summer obtained from the 2DFFT analysis of the

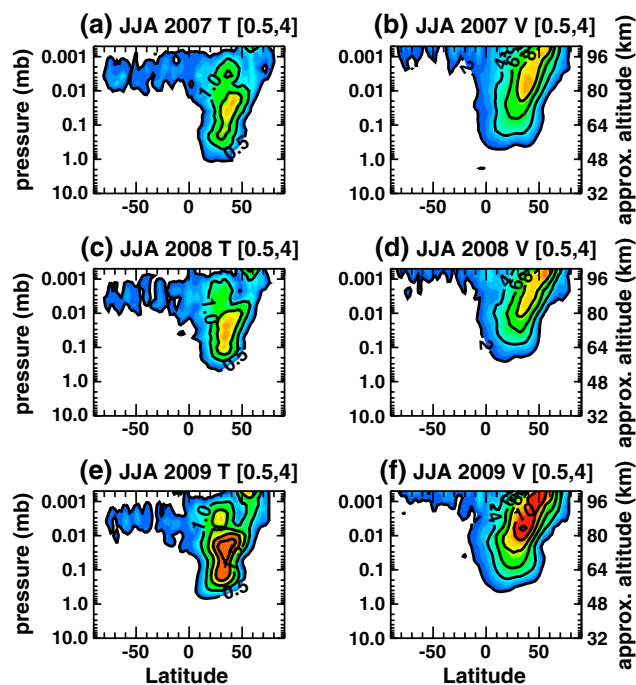


Figure 5. As in Figure 4 but for the [0.5,4] Q2DW component.

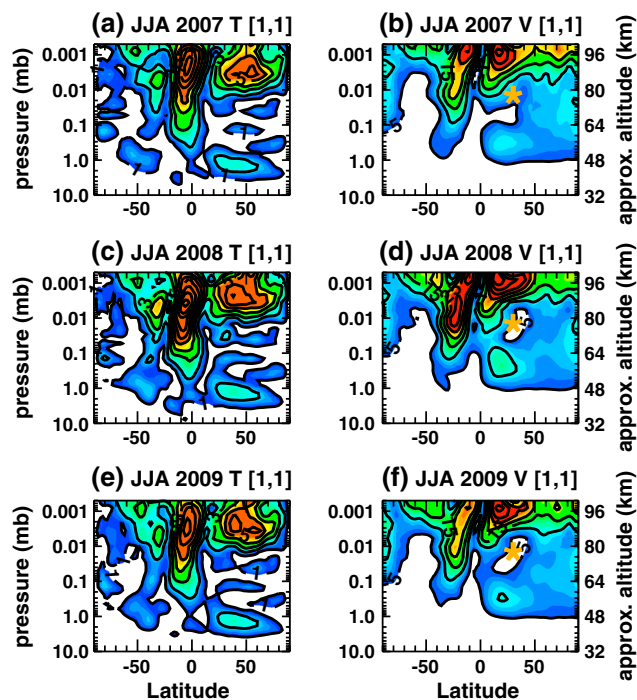
structure in this background temperature gradient throughout the NH summer MLT region. Specifically, maxima in the [0.5,3] temperature amplitude near 0.02 hPa and 0.001 hPa in Figure 4 occur where the meridional gradients in zonal mean temperature are most pronounced; the minimum in the Q2DW temperature amplitude between 0.01 and 0.002 hPa occurs where the meridional temperature gradient is relatively weak.

Figure 5 plots the JJA mean amplitudes of the [0.5,4] component in NOGAPS-ALPHA temperatures and meridional winds. While the latitude and altitude dependences of the [0.5,4] temperature component are similar to the [0.5,3] component, we find that the peak values of [0.5,4] in temperature are located on average  $\sim 5^\circ$  equatorward and  $\sim 10\text{--}12$  km lower than the location of the [0.5,3] temperature peaks. Peak values of the [0.5,4] meridional wind response are also shifted equatorward by  $\sim 5^\circ$ , on average, relative to the peak [0.5,3] wind values. One main difference between the zonal wave number 3 and 4 features, however, is that the [0.5,4] meridional wind amplitudes do not exhibit the sharp increase with height seen in the [0.5,3] wind amplitudes. Another important difference is that, on average, both the peak temperature and wind amplitudes of [0.5,4] are 30% less than the amplitudes of [0.5,3].

We note here that *Tunbridge et al.* [2011] found evidence for a westward zonal wave number 2 feature associated with the Q2DW in NH summer based on analysis of MLS temperatures from 2004 to 2009. Our 2DFFT analysis of NOGAPS-ALPHA temperatures finds that peak amplitudes for this [0.5,2] component are typically less than 1.5 K and, unlike the zonal wave 3 and 4 cases, are found over a broad latitude region from  $10^\circ\text{N}$  to  $70^\circ\text{N}$  above  $\sim 80\text{km}$ . The latitude and altitude dependences of the [0.5,2] component in meridional wind (not shown) are also markedly different from the zonal wave number 3 and 4 cases, showing peak values of  $\sim 10\text{ m s}^{-1}$  throughout the upper mesosphere centered over the equator. Because this apparent wave number 2 Q2DW exhibits spatial characteristics that are fundamentally different from [0.5,3] to [0.5,4] results, the present study will focus on the dynamical factors controlling the growth and evolution of wave number 3 and 4 components of the Q2DW in NH summer. Possible relationships between these components and the zonal wave number 2 Q2DW will be examined in a future study.

One distinct advantage of 6-hourly global HDAS output is the ability to discriminate among the diurnal migrating (or [1,1]) tide and the [0.5,3] and [0.5,4] components of the Q2DW. As discussed in section 1, there is both theoretical and observational evidence of mutual interaction between the Q2DW and the migrating diurnal tide. Most of these studies, however, focus on the SH summer period when Q2DW amplitudes are larger than during NH summer. We next examine the general characteristics of the [1,1] tide obtained from the 2DFFT analysis for June–August of 2007–2009.

A comparison of the spatial structure of the JJA mean [0.5,3] temperature and meridional wind components in Figure 4 shows that the Q2DW in meridional wind does not exhibit the two distinct peaks near 75 km and 90 km seen in the temperature Q2DW. Instead, the amplitude of the meridional wind Q2DW increases steadily with altitude and peaks at 90 km. The spatial structure of the meridional wind Q2DW in Figure 4 is consistent with the interpretation of the Q2DW as a global normal mode, which grows with altitude as atmospheric density decreases until vertical propagation is limited by, e.g., the presence of a critical line where the background wind speed equals the phase speed of the wave. The Q2DW in temperature arises from meridional parcel displacements superimposed upon a background meridional gradient in zonal mean temperature, and the double peak in the temperature Q2DW is produced by the vertical struc-



**Figure 6.** As in Figure 4 but for the [1,1] migrating diurnal tide. Contour intervals are 1 K and 5 m s<sup>-1</sup>. Symbols indicate region of peak [0.5,3] Q2DW amplitudes in temperature near 75 km in Figure 4.

variations in the strength of tidal forcing (i.e., latent heat release and ozone heating), and variations in the strength of the zonal winds in MLT. The latter is highly dependent on gravity wave drag, and wind variations in the stratosphere can act as a filter for upward propagating gravity waves. An analysis of TIMED Doppler Interferometer winds from 2002 to 2007 by *Wu et al.* [2008] found that amplitudes of the migrating diurnal tide tend to be larger during the westerly phase of the stratospheric quasi-biennial oscillation (QBO). We note that the QBO was in its easterly phase during July 2007; during July 2008 and 2009, winds in the equatorial lower stratosphere were westerly. Therefore, it does not appear that the QBO can explain the interannual variations in the Northern subtropical tidal amplitudes shown in Figure 6. Although the origins of the interannual variability in the diurnal tide are currently not understood, the JJA mean Q2DW amplitudes and diurnal tide in Figures 4–6 are consistent with the interpretation that larger tidal amplitudes can limit the growth of the Q2DW. We examine the relationship between the Q2DW and migrating diurnal tide in more detail in section 3.3.

### 3.2. Intraseasonal Variability of the Q2DW

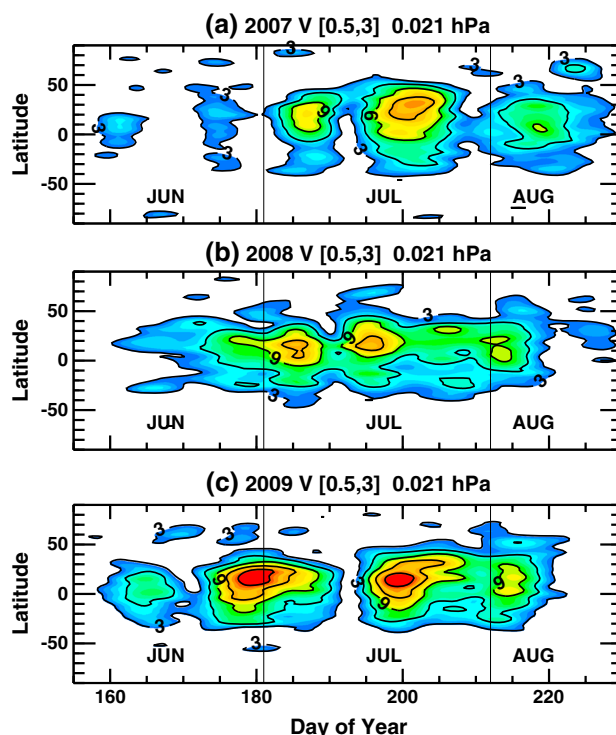
We next examine the variability of the [0.5,3] and [0.5,4] components over the course of each summer period (June–August). As described in section 2, this is done by applying a band-pass filter at zonal wave numbers 3 and 4 to the inverse 2-D Fourier transform of the NOGAPS-ALPHA fields over a 75 day interval from 5 June to 20 August of each year. To facilitate comparisons with Q2DW variability seen in the SH summer reported by *McCormack et al.* [2010], we will focus on the seasonal evolution of the Q2DW during NH summer in NOGAPS-ALPHA meridional wind fields. We note that the time behavior of both the Q2DW and diurnal tide in temperature during NH summer (not shown) closely matches the time behavior of these features in meridional wind.

Figure 7 plots [0.5,3] amplitudes in meridional wind at 0.02 hPa (~ 75 km) as a function of latitude and time throughout the NH summers of 2007–2009. In all three cases, the [0.5,3] amplitudes peak shortly after solstice and then again 15–20 days later. There is also evidence of a weaker third peak in August. Our analysis of the three JJA periods finds the largest [0.5,3] amplitude of 17 m s<sup>-1</sup> occurs during 2009, which is consistent with the larger mean JJA amplitudes in both temperature and pressure during 2009 in Figure 4.

Figure 8 plots the [0.5,4] meridional wind amplitude at 0.02 hPa for the NH summers of 2007–2009. The time behavior of the wave number 4 Q2DW differs from the behavior of wave number 3 in that there are

Figure 6 plots the mean [1,1] RMS amplitudes in both temperature and meridional wind for JJA 2007–2009. The latitude and altitude structure of the tidal amplitudes derived from NOGAPS-ALPHA fields are quite similar from year to year, and are in good agreement with earlier modeling studies [e.g., *Norton and Thuburn, 1999; Chang et al., 2011*]. At 0.02 hPa and 40°N, where the [0.5,3] temperature amplitudes are large (as indicated by the symbols in Figure 6b, 6d, and 6f), the JJA mean [1,1] amplitudes in meridional wind are greater in 2007 than in either 2008 or 2009. The larger [1,1] meridional wind amplitudes in JJA 2007 at this location coincide with relatively smaller Q2DW amplitudes observed during JJA 2007.

As noted in section 1, larger amplitudes of the migrating diurnal tide can limit the growth of the Q2DW. The interannual variations in tidal amplitudes seen in Figure 6 can be caused by a variety of different factors, including



**Figure 7.** Latitude–time section of [0.5,3] Q2DW amplitudes in meridional wind at 0.02 hPa for the June–August period of (a) 2007, (b) 2008, and (c) 2009. Contour interval is  $3 \text{ m s}^{-1}$ .

able to distinguish among different wave number components of the Q2DW. Offermann *et al.* [2011] also reported a peak in Q2DW temperature amplitudes in April, giving rise to an apparent triple-peak structure throughout the NH spring–summer period. Presently, NOGAPS-ALPHA fields for NH spring are only available for the years 2008 and 2009. Our analysis of temperature and horizontal winds does not find evidence for Q2DW activity during April or May of 2008 and 2009. The study by Tunbridge *et al.* [2011] also found no significant Q2DW signal in MLS temperatures at 91 km during spring of 2008 and 2009 [Tunbridge *et al.*, 2011, Figure 4]; however, Tunbridge *et al.* [2011] did report Q2DW temperature amplitudes of 2–3 K in spring of 2006. Since the study by Offermann *et al.* [2011] reports Q2DW amplitudes averaged over several years (e.g., 2005–2009), it is not possible to evaluate this apparent interannual variability in the NH spring Q2DW from their OH temperature measurements. Future studies that involve direct comparisons between NOGAPS-ALPHA fields and independent ground-based observations on a year-by-year basis throughout NH spring and summer would clarify this issue.

### 3.3. Intraseasonal Variability of the Migrating Diurnal Tide

The results in section 3.1 show that over the three NH summers examined, the largest Q2DW amplitudes occur in 2009, when the amplitudes of the diurnal tide are smallest. Earlier observational studies of the Q2DW during SH summer [e.g., Lima *et al.*, 2004; Pancheva, 2006; Hecht *et al.*, 2010] found an inverse relationship between the amplitudes of the Q2DW and the migrating diurnal tide. As discussed in section 1, one explanation for this relationship is that larger diurnal tidal amplitudes can locally reinforce the Q2DW, which promotes instability and wave breaking that effectively limit the amplification of the Q2DW. Another explanation is that when Q2DW amplitudes are large, nonlinear interactions can take place between the [0.5,3] and [1,1] “parent” waves that produce “child” waves whose frequency/wave number characteristics are determined from combinations of the sums and differences of the parent waves. In this scenario, the cascade of energy to smaller scales causes the amplitude of the child waves to grow at the expense of the diurnal tide, producing anticorrelation between the Q2DW and diurnal tide shortly after summer solstice.

Numerous modeling studies have documented this latter process in both NH and SH summer [Norton and Thuburn, 1999; Palo *et al.*, 1999; Chang *et al.*, 2011], as evidenced by rapid enhancement of the Q2DW along with a simultaneous decrease of  $\sim 20\%$  in the amplitude of the diurnal tide and the emergence of spectral

several peaks in amplitude throughout the summer period from late June to mid-August. For example, [0.5,4] wind amplitudes of  $12 \text{ m s}^{-1}$  occur in August of 2007 and 2009, while in 2008 the maximum amplitude of  $15 \text{ m s}^{-1}$  occurs in mid-July. As with the [0.5,3] amplitudes in Figure 7, the largest [0.5,4] amplitudes at this level also occur during JJA 2009. Overall, the meridional extent of the peak [0.5,4] amplitudes for all three summers at this level is narrower in latitude than for the [0.5,3] amplitudes in Figure 7.

The two peaks in the [0.5,3] amplitudes following solstice are consistent with the results in Tunbridge *et al.* [2011, Figure 10c]. This is to be expected, since NOGAPS-ALPHA assimilates the same MLS temperature observations (in addition to SABER temperature observations). Offermann *et al.* [2011] found similar behavior of the Q2DW from upper mesospheric OH temperature measurements at  $51^\circ \text{N}$  during 2004–2009, i.e., two peaks in Q2DW amplitude in early and late NH summer, although this study was not

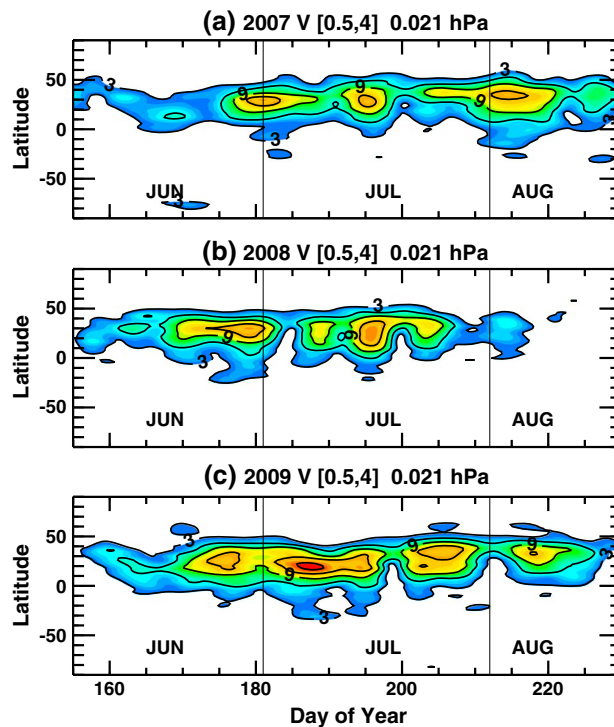


**Figure 8.** As in Figure 7 but for the [0.5,4] Q2DW amplitudes.

meridional wind between 20°N and 40°N were comparatively weak during July 2007 (Figure 7a), corresponding [1,1] amplitudes were comparatively strong, exceeding 5 m s<sup>-1</sup> throughout much of the NH subtropics. The larger [0.5,3] amplitudes in July of 2008 and 2009 (Figures 7b and 7c, respectively) occur when tidal amplitudes were comparatively weaker (less than 5 m s<sup>-1</sup>) throughout the NH subtropics.

While the results in Figure 9 confirm the inverse relationship between the Q2DW and diurnal tide from 1 year to the next at ~75 km, there is no indication of correlation between the Q2DW and tide within an individual season that would indicate the presence of any type of mutual, nonlinear interaction. As noted above, this process has generally been found to occur at higher altitudes in the subtropical regions where the amplitudes of both the Q2DW and tide are much larger than they are at 75 km. To further investigate the possibility of nonlinear Q2DW-tide interactions in NH summer, we have compared the intraseasonal variability of the [1,1], [0.5,3] and [0.5,4] components in meridional wind over a range of NH latitudes from 0.1 to 0.002 hPa. As an example, Figure 10 plots time series of the [0.5,3], [0.5,4], and [1,1] amplitudes derived from the 2DFFT analysis at 30°N and 0.0036 hPa (~88 km) over the JJA periods of 2007–2009. This level is chosen for the comparison based on the study by McCormack *et al.* [2010], which found anticorrelation between the [1,1] and [0.5,3] components of NOGAPS-ALPHA meridional winds in the SH summer at 0.0036 hPa and 30°S latitude and a resulting [1,6] “child-wave” signature indicative of nonlinear interactions between the diurnal tide and Q2DW. To determine if such behavior is evident in the NH summer MLT region, we focus in particular on the month of July when the [0.5,3] amplitudes are generally largest.

As Figure 10 indicates, there is no evidence of a strong anticorrelation between [1,1] and either [0.5,3] or [0.5,4] at this location to indicate that the larger Q2DW amplitudes in 2008 or 2009 result from the Q2DW growing at the expense of the diurnal migrating tide via nonlinear wave-wave interaction. Similar analysis at other pressure levels and latitudes throughout the NH summer MLT (not shown) confirms this result. We also find no signature of the [1,6] or other child waves in the power spectra of the wind fields that would indicate Q2DW-tidal interactions. Instead, we find periods of both correlation and anticorrelation between the [0.5,3] and [0.5,4] components of the Q2DW, most notably during July of 2007 and 2009, suggesting that in some circumstances conditions may favor growth of both Q2DW modes, while in other circumstances one component of the Q2DW may be growing preferentially over another.

Overall, the lack of a strong anticorrelation between the Q2DW and migrating diurnal tide within the individual seasons (illustrated in Figure 10) indicates that year-to-year variability in the background state of the NH

peaks in the meridional wind field at harmonics of the diurnal cycle at subtropical latitudes near 90 km. To determine whether the observed interannual variability in the Q2DW over the three NH summers can be attributed to possible Q2DW-tidal interactions, we now examine the temporal variability of the [1,1] amplitudes in meridional wind in relation to the Q2DW.

Figure 9 plots the [1,1] meridional wind amplitude as a function of latitude and time at the 0.02 hPa level (~75 km) for the NH summer period of 2007–2009. The [1,1] signal is largely confined to the subtropical regions of each hemisphere, which is consistent with earlier studies [e.g., Norton and Thuburn, 1999; Wu *et al.*, 2008; Lieberman, 1999; Chang *et al.*, 2011]. In all 3 years, the tidal amplitudes are at a minimum near solstice and tend to increase as the summer progresses. A comparison of Figures 7 and 9 shows that when [0.5,3] amplitudes in meridional

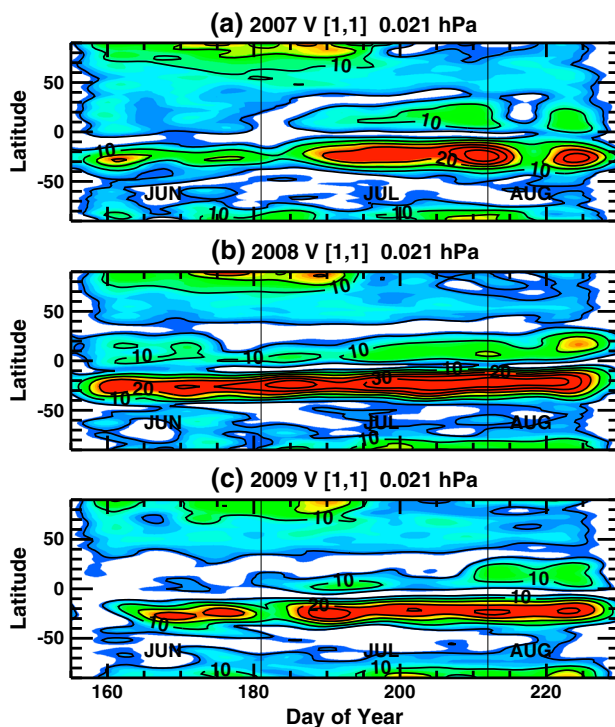


**Figure 9.** Latitude–time section of [1,1] tidal amplitudes at 0.02 hPa for the June–August period of (a) 2007, (b) 2008, and (c) 2009. Contour interval is  $10 \text{ m s}^{-1}$ .

using daily stratospheric meteorological fields. In the present work, we extend this type of analysis into the upper mesosphere using global synoptic NOGAPS-ALPHA wind and temperature fields.

A necessary condition for the growth of the Q2DW in the summer extratropical mesosphere via baroclinic instability is a reversal of the meridional gradient in zonal mean quasi-geostrophic potential vorticity  $\bar{q}_\phi$  [see, e.g., Plumb, 1983; Pfister, 1985]. In spherical coordinates this is computed from the relation

$$\bar{q}_\phi = \frac{2\Omega}{a} \cos\phi - \frac{1}{a} \frac{\partial}{\partial\phi} \left[ \frac{1}{\cos\phi} \frac{\partial(\bar{u}\cos\phi)}{\partial\phi} \right] - (2\Omega\sin\phi)^2 e^{z/H} \frac{\partial}{\partial z} \left[ \frac{1}{N^2} e^{-z/2H} \frac{\partial\bar{u}}{\partial z} \right] \quad (1)$$

where  $\phi$  is latitude,  $\bar{u}$  is the zonal mean zonal wind speed,  $H$  is the scale height,  $z$  is the log-pressure vertical coordinate,  $N$  is the Brunt-Vaisälä frequency,  $a$  is the Earth’s radius, and  $\Omega$  is the planetary rotation rate. As equation (1) shows, reversals in  $\bar{q}_\phi$  (i.e., from positive to negative values) are determined by the curvature in the background zonal wind distribution. Consequently, accurate wind analyses are needed to diagnose baroclinic instability. Here we use global NOGAPS-ALPHA horizontal wind and temperature fields on constant pressure surfaces to compute  $\bar{q}_\phi$  during July of 2007, 2008, and 2009, when the [0.5,3] amplitudes tend to be largest. This information shows how variations in baroclinic instability from one NH summer to the next may help to explain the observed interannual variations in the Q2DW amplitudes shown in Figures 4 and 5. While reversal of  $\bar{q}_\phi$  is a necessary condition for Q2DW growth through baroclinic instability, it is not sufficient. Conditions must also support the growth of the disturbance in the absence of a critical line.

Theory states that growth of the Q2DW is related to EP flux divergence in baroclinically unstable regions [e.g., Plumb, 1983]. The EP flux vector can be computed from the eddy heat and momentum fluxes associated with the Q2DW using the relation

$$\mathbf{F}[\phi, z] = \rho \cos\phi \left[ -\overline{u'v'} \right], \left( f - \frac{1}{\cos\phi} [\bar{u} \cos\phi]_\phi \right) \frac{R}{HN^2} \overline{v'T'} \right]. \quad (2)$$

where  $\rho$  is density,  $f$  is the Coriolis parameter, and  $R$  is the gas constant for dry air. The terms  $\overline{u'v'}$ , and  $\overline{v'T'}$  represent zonal mean eddy momentum and heat fluxes (overbars represent zonal means, primes denote deviations from the zonal mean, and brackets denote a daily average). These quantities are computed from gridded 6-hourly NOGAPS-ALPHA zonal wind, meridional wind, and temperature fields that

summertime mesosphere, rather than amplification of the Q2DW due to interaction with the tides, could be responsible for the interannual differences in the amplitudes of the Q2DW seen in Figures 4 and 5. In the following section, we use the NOGAPS-ALPHA meteorological analyses to examine how variations in the background state affects the origin and growth of the Q2DW in NH summer.

#### 4. EP-Flux Diagnostics

In this section, we employ a series of diagnostic calculations to examine the origin and growth of the Q2DW in the NH summer based on linear quasi-geostrophic theory. Such an approach has been used previously to study the behavior of the Q2DW near the stratopause [Randel, 1994; Orsolini et al., 1997; Limpasuvan et al., 2000] and identify regions of baroclinic and/or barotropic instability favoring Q2DW growth and propaga-

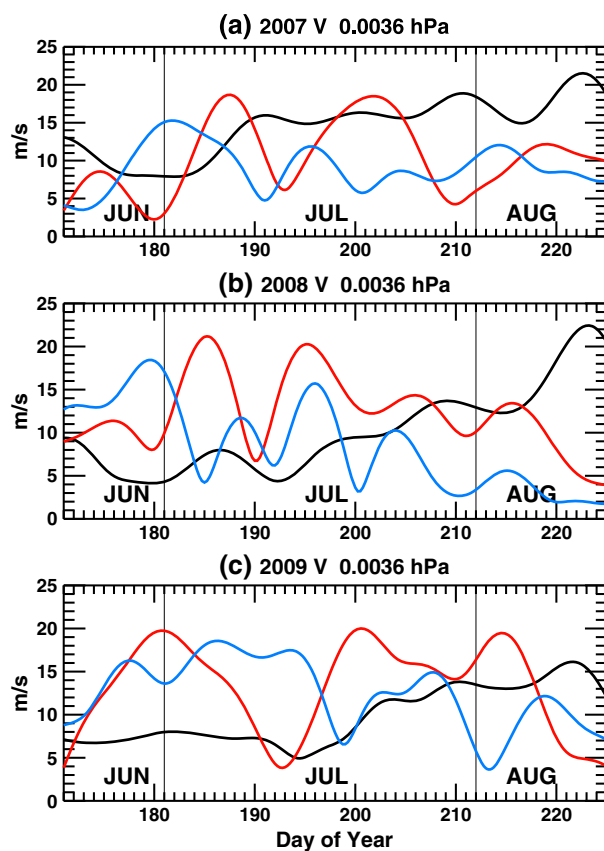


**Figure 10.** Time series of the [0.5,3] (red), [0.5,4] (blue), and [1,1] (black) amplitudes at 30°N and 0.0036 hPa during June–August of (a) 2007, (b) 2008, and (c) 2009.

have been band-pass filtered in order to isolate the [0.5,3] or [0.5,4] components of the Q2DW, as described in section 2.

Although numerous modeling studies have examined EP flux-based diagnostics of the Q2DW, only a few studies have used observations to calculate EP fluxes associated with the Q2DW. For example, *Lieberman* [1999] used High Resolution Doppler Imager (HRDI) wind and temperature observations from January 1994 to compute EP flux divergences in the SH summer mesosphere. The study by *Offermann et al.* [2011] used geostrophic winds derived from MLS temperature measurements to relate the occurrence of baroclinically unstable conditions to the intraseasonal variability in the Q2DW observed from ground-based stations in northern Europe. Similarly, *Ern et al.* [2013] used wind information derived from SABER temperatures to investigate forcing of the Q2DW by gravity wave activity. Here we use output from the NOGAPS-ALPHA global HDAS to describe EP flux divergence associated with both [0.5,3] and [0.5,4] components of the Q2DW in the NH summer.

Figure 11 plots EP flux vectors related to the [0.5,3] Q2DW for three cases: 20 July 2007 (Figure 11a), 16 July 2008 (Figure 11b), and 23 July 2009 (Figure 11c). These three cases were chosen based on the large Q2DW amplitudes observed on these dates (see Figure 7). Also plotted in Figure 11 is the daily average zonal mean zonal wind distribution for these days, from which we calculate values of  $\bar{q}_\phi$ . To illustrate the relationship between baroclinically unstable regions and Q2DW growth, shaded regions in Figure 11 indicate where  $\bar{q}_\phi$  is negative. In all three cases, Figure 11 shows EP flux divergence related to the [0.5,3] component of the Q2DW near the core of the easterly jet between 0.05 and 0.1 hPa. The direction of the EP flux vectors indicate propagation of wave activity away from the approximate location of the critical line for the [0.5,3] wave, which is indicated by the bold red contour. In the lower mesosphere the propagation is primarily equatorward, while in the upper mesosphere it is primarily poleward and upward. We note that the regions of high vertical EP flux in Figure 11 coincide with the location of the local maxima in the [0.5,3] temperature amplitudes in Figure 4. This indicates that the temperature Q2DW near ~75 km and 40°N may be triggered by baroclinic instability near the jet core. We explore this possibility further in section 5 with the use of a linear instability model that uses the NOGAPS-ALPHA assimilated winds and temperatures as input.

Figure 12 plots the EP fluxes of the Q2DW for three cases when [0.5,4] amplitudes peaked during the three NH summers: 4 August 2007 (Figure 12a), 22 June 2008 (Figure 12b), and 4 July 2009 (Figure 12c). Wave activity associated with the [0.5,4] component originates just equatorward of the easterly jet core between 0.1 and 0.2 hPa and propagates away from the estimated location of the critical line (blue contour in Figure 12), mainly in the upward and poleward direction. It is interesting to note how the locations of the critical lines in Figures 11 and 12, which are determined by the curvature of the zonal mean zonal wind, can affect the upward propagation of the Q2DW. For example, in the 2007 case (Figure 11a) the summer easterly jet is weaker and exhibits a poleward tilt with increasing altitude between 40°N and 65°N, which leads to a gradual sloping of the critical lines upward and poleward, away from the source regions. In the 2008

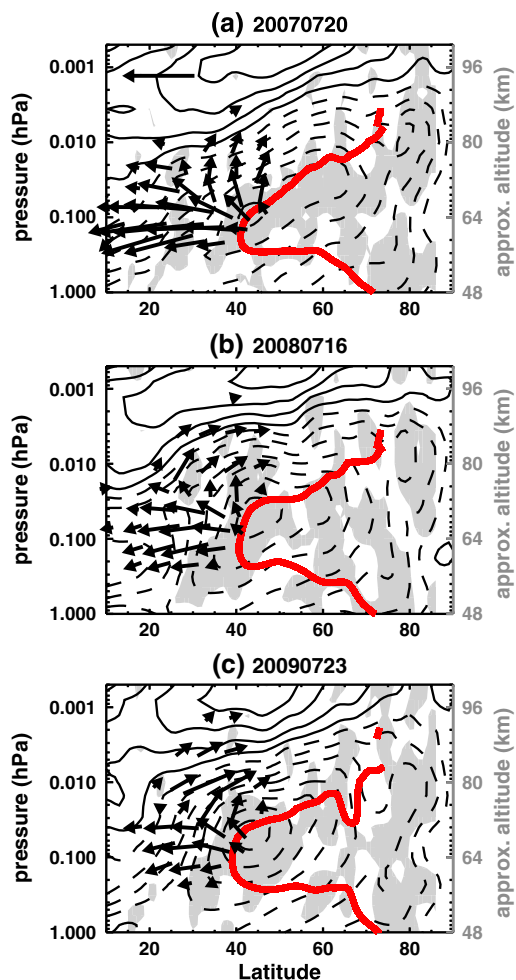


**Figure 11.** Contour plots of daily averaged NOGAPS-ALPHA zonal mean zonal winds for (a) 20 July 2007, (b) 16 July 2008, and (c) 23 July 2009. Contour interval is  $10 \text{ m s}^{-1}$ ; dashed contours represent easterly winds. Shaded regions indicate where meridional gradient in quasi-geostrophic potential vorticity is negative. Red contour indicates location of critical line for [0.5,3] Q2DW. Arrows represent EP-fluxes associated with the [0.5,3] Q2DW. For reference, Figure 11a includes a vector whose length equals  $10^5 \text{ kg m}^{-2}$ .

from the source region that allows upward wave activity to spread throughout a much wider area. Figure 14 summarizes this relationship, plotting time series of the zonal mean zonal winds at  $40^\circ\text{N}$  and 0.02 hPa from 15 May to 31 August of 2007, 2008, and 2009. Focusing on the month of July, the zonal mean easterly flow was strongest in 2009, when the [0.5,3] Q2DW amplitudes were largest. During July 2007, when Q2DW amplitudes were smallest, the zonal mean easterlies peaked briefly in early July and remained relatively weak thereafter.

The EP-flux diagnostics based on the NOGAPS-ALPHA meteorological fields indicate that the Q2DW originates from baroclinic instabilities near the equatorward flank of the mesospheric summer easterly jet. The interannual variability of the Q2DW amplitudes in NH summer over the 2007–2009 period closely follows interannual variability in the strength and position of the summer easterly jet core, which determines the locations of the critical lines for the [0.5,3] and [0.5,4] components of the Q2DW. As the results in section 3 show, both wave number 3 and wave number 4 components of the Q2DW are of comparable magnitude in NH summer, and they both exhibit a high degree of variability throughout the summer season. In the next section, we use a linearized instability model to examine this intraseasonal variability in more detail.

and 2009 cases, the jet is stronger and its core is centered between  $40^\circ\text{N}$  and  $50^\circ\text{N}$ , producing a “bull-nose” shape in the location of the critical lines where the equatorward edge of the critical lines extends higher in altitude than in the 2007 case. In particular, the higher extent of the critical lines in the 2009 case (see Figure 11c and Figure 12c) appears to direct more Q2DW activity upward into the region above the 0.01 hPa level.

To further examine the relationship between the location of the Q2DW critical line and vertical wave propagation during NH summer, Figure 13 plots the time evolution of zonal mean zonal winds over the NH extratropics during July of 2007, 2008, and 2009 at 0.02 hPa. Superimposed upon the wind contours are regions where  $\bar{q}_\phi$  is negative (gray shading). Also plotted in Figure 13 are values of the [0.5,3] eddy heat flux (heavy black contours), which are proportional to the vertical component of the EP-flux (equation 2). During July 2007 (Figure 13a), the location of the [0.5,3] critical line retreats poleward as the month progresses due to the weakening easterly jet. In contrast, the stronger easterly jet during July 2008 and 2009 (Figures 13b and 13c) maintains the position of the [0.5,3] critical line near  $40^\circ\text{N}$  throughout the month. As a result, there are more sustained periods of high eddy heat flux during July 2008 and 2009.

These results indicate that the larger Q2DW amplitudes in July during 2008 and 2009 as compared to July 2007 can be attributed to the characteristics of the summer easterly jet. Specifically, a stronger and more defined jet structure near the Q2DW source region acts to focus more wave activity upward through a smaller area by nature of the critical line’s location. A weaker jet, on the other hand, results in the critical line sloping away

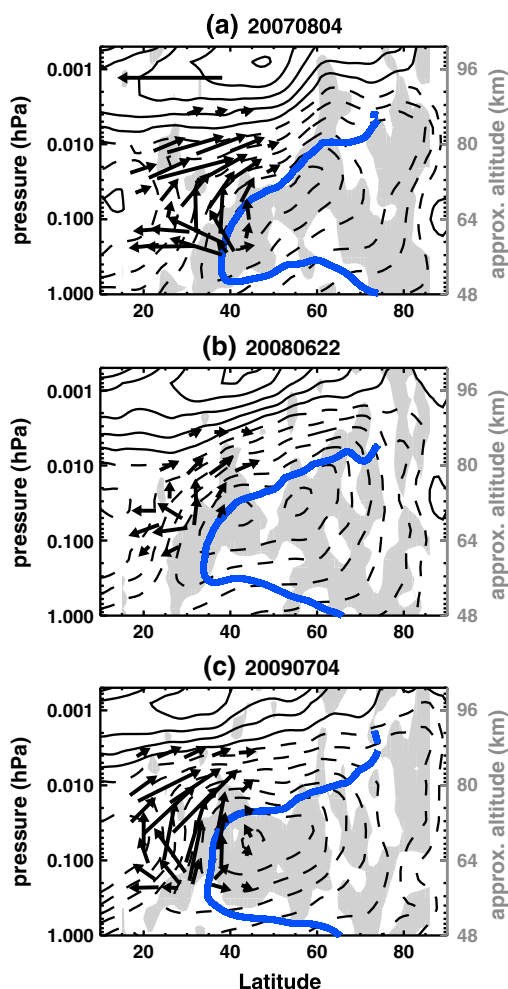


**Figure 12.** Contour plots of daily averaged NOGAPS-ALPHA zonal mean zonal winds for (a) 4 August 2007, (b) 22 June 2008, and (c) 4 July 2009, as in Figure 11. Blue contour indicates location of critical line for [0.5,4] Q2DW. Arrows represent EP-fluxes associated with the [0.5,4] Q2DW. For reference, Figure 12a includes a vector whose length equals  $10^5 \text{ kg m}^{-2}$ .

### 5. Instability Model Results

The results in the preceding sections show that both wave number 3 and wave number 4 components of the Q2DW arise from baroclinically unstable regions near the summer easterly jet at midlatitudes in the NH mesosphere. As Figures 7 and 8 illustrate, amplitudes of the [0.5,3] component are typically largest in July, while amplitudes of the [0.5,4] component peak intermittently throughout the period from late June to mid-August. This variability is consistent with an earlier study of the NH Q2DW by *Tunbridge et al.* [2011], which showed that in some years the amplitude of the [0.5,4] component surpasses the amplitude of the [0.5,3] component in August.

To better understand the origins of this behavior, we use a simple linear instability model to examine the characteristics of the fastest-growing unstable modes in the MLT region near the NH summer easterly jet. This approach has been used to study other types of free traveling planetary waves in the MLT [e.g., *Hartmann*, 1983; *Manney and Randel*, 1993]. The model is based on the linearized quasi-geostrophic potential vorticity equation for frictionless, adiabatic flow on a  $\beta$ -plane centered at midlatitudes [see, e.g., *Andrews et al.*, 1987, equation 3.4.5]:

$$q'_t + \bar{u}q'_x + v'\bar{q}_y = 0. \tag{3}$$

Here the potential vorticity is derived from the NOGAPS-ALPHA horizontal wind fields. Formulating the zonal wind and potential vorticity distributions in terms of the geostrophic stream function and assuming periodic solutions as functions of both longitude and time allows equation (3) to be cast as an eigenvalue problem of the form

$$\mathbf{Ax} = c\mathbf{Bx} \tag{4}$$

where  $\mathbf{x}$  is the state vector represented by gridded values of the stream function and the complex phase speed  $c$  is the eigenvalue. The operator  $\mathbf{A}$  is determined from  $\bar{u}$  and  $\bar{q}_y$ , the operator  $\mathbf{B}$  is determined from the finite-differenced potential vorticity equation; both  $\mathbf{A}$  and  $\mathbf{B}$  depend on the zonal wave number.

To simplify the calculation, the daily averaged values of NOGAPS-ALPHA zonal wind fields are subsampled onto the instability model domain, which consists of a uniform grid with 20 points in latitude extending from 20°N to 60° N latitude and 26 points in altitude extending from 65 to 90 km. For a given day,  $\mathbf{A}$  and  $\mathbf{B}$  are constructed from the geostrophic stream function and potential vorticity using these subsampled daily averaged zonal winds. Standard numerical codes are then used to solve the eigenvalue problem and obtain  $\mathbf{x}$  (i.e., the wave modes) and  $c$  (i.e., phase speeds) for zonal wave numbers 1 through 6. The fastest growing modes are evaluated in terms of their  $e$ -folding times, which are determined from the inverse of the imaginary component of the phase speed for each zonal wave number. The periods of the unstable modes are determined from the real component of the phase speed (positive values indicate westward propagation). In addition, each mode's spatial structure contains wind and temperature information from which EP fluxes can be computed.

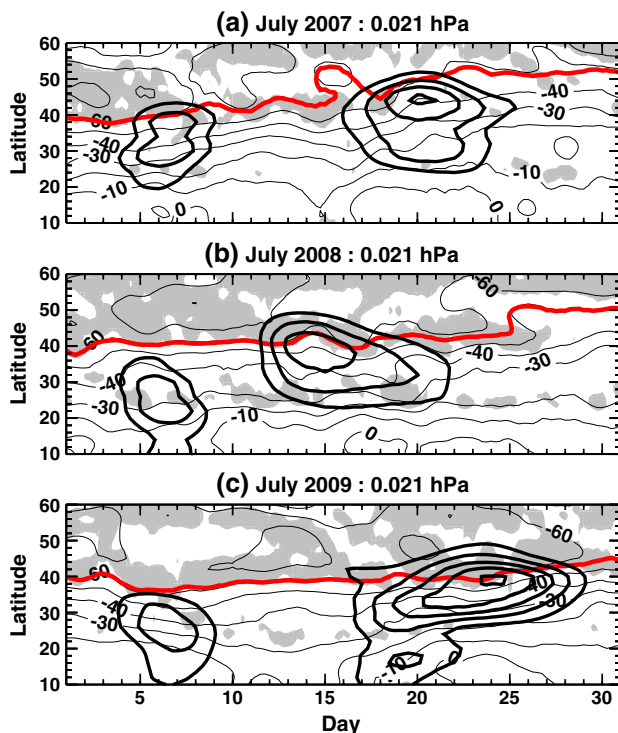


**Figure 13.** Latitude-time sections of daily averaged NOGAPS-ALPHA zonal mean zonal winds at 0.02 hPa during July of (a) 2007, (b) 2008, and (c) 2009. Shaded regions indicate where meridional gradient in quasi-geostrophic potential vorticity is negative. Red contour indicates approximate location of critical line for [0.5,3] Q2DW. Heavy black contours indicating positive [0.5,3] Q2DW eddy heat flux are drawn at values of 10, 15, 20, 25  $\text{K m s}^{-1}$ .

the fastest-growing modes are again at zonal wave numbers 3–5 (Figure 16b). However, the *e*-folding times of 3–4 days are much shorter than the July case. The spatial structure of the waves in this case now exhibits two maxima (Figures 16c–16e) centered near 35°N and 45°N. For this August case, the zonal wave number 3 (Figure 16e) solution has a period of 3.1 days and the wave number 4 solution has a period of 2.3 days.

The results from these two cases show that the growth time of the Q2DW decreased by a factor of 2–3 between early July and early August 2009. To determine if this is a systematic effect, the stability model was applied to daily average NOGAPS-ALPHA zonal wind fields throughout the period from 5 June to 10 August 2009. Figure 17 plots the resulting values of the period and growth time for both wave number 3 and 4 solutions.

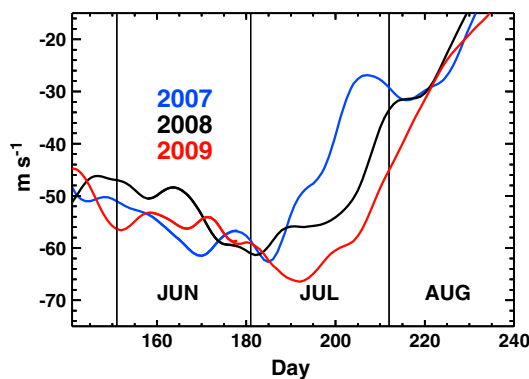


**Figure 14.** Time series of zonal mean zonal wind speed at 40°N and 0.02 hPa during NH summer of 2007 (blue curve), 2008 (black curve), and 2009 (red curve).

In this discussion, we focus on the summer of 2009 when the Q2DW was most prominent. We first examine model output for two individual cases: 10 July and 5 August. These cases were chosen to highlight the development of the [0.5,3] and [0.5,4] components of the Q2DW, respectively, during the NH summer of 2009. Figure 15a plots the zonal wind and  $\bar{q}_y$  distributions over the model domain for the 10 July case. We find that zonal wave numbers 3–5 exhibit the fastest growth rates, with *e*-folding times of ~8–9 days (Figure 15b). The normalized stream function amplitudes of waves 1–4 (Figure 15c–15e) maximize in the region between 30°N and 40°N and 60–70 km, which closely resembles the observed spatial structure of the [0.5,3] temperature Q2DW in Figure 4. In general, the period of the fastest-growing modes decreases with increasing horizontal scale. On this particular day, the zonal wave number 3 (Figure 15e) solution has a period of 2 days, and the wave number 4 solution has a period of 1.5 days.

Figure 16 plots instability model results for the 5 August 2009 case. We find that the *e*-folding times of 3–5 (Figure 16b). However, the *e*-folding times of 3–4 days are much shorter than the July case. The spatial structure of the waves in this case now exhibits two maxima (Figures 16c–16e) centered near 35°N and 45°N. For this August case, the zonal wave number 3 (Figure 16e) solution has a period of 3.1 days and the wave number 4 solution has a period of 2.3 days. For plotting purposes, these time series have been smoothed using a three-point running average. During much of June and early July, both wave numbers have periods near 2 days (Figure 17a). Starting in mid-July, the periods increase sharply and then vary in the 3–7 day range thereafter. By late summer, the period of wave number 4 is consistently 1–2 days shorter than wave number 3. The growth time of wave number 4 is shorter than wave number 3 throughout most of the summer (Figure 17b), and the growth times of wave numbers 3 and 4 both decrease sharply during late July and early August.

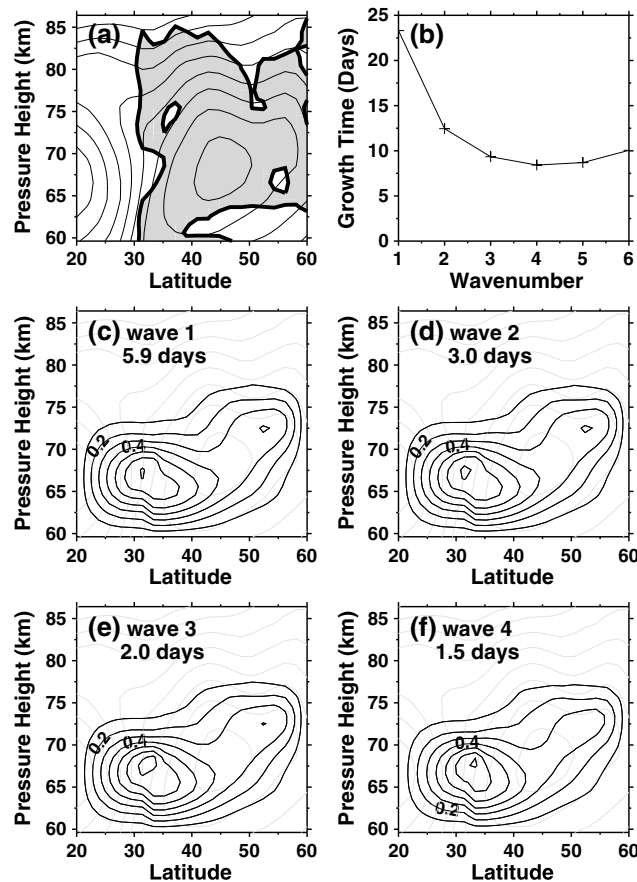


**Figure 15.** Linear instability model results for 10 July 2009 case. (a) Latitude-altitude distribution of zonal winds (contour interval of  $10 \text{ m s}^{-1}$ ), shaded regions indicate where  $q_y < 0$ ; (b) e-folding times for westward propagating unstable modes as function of zonal wave number; (c–f) normalized amplitudes of the geostrophic stream function solutions, and the period of each solution, for wave numbers 1 through 4.

based on the observational and model results presented here, we speculate that one possible explanation for this behavior may be that the faster growing wave number 4 unstable mode tends to emerge initially in June, only to be overtaken by the slower growing wave number 3 mode. When the Q2DW amplitudes and associated EP fluxes grow large enough to become unstable and dissipate, they modify the vertical shear structure in the background zonal wind such that it no longer produces fast-growing unstable modes at zonal wave numbers 3 and 4 with periods near 2 days. This would be consistent with the sudden increase in the period of the unstable wave 3 and wave 4 modes in mid-July 2009 (Figure 17a). As baroclinically unstable regions near the easterly jet reform after the Q2DW dissipates, another fast-growing zonal wave 4 mode can emerge in late July or early August. However, by this time the effects of a weakening easterly jet (Figure 14) and increasing tidal amplitudes (Figure 9) will combine to limit growth of the slower [0.5,3] mode. Fully interactive GCM simulations are needed to test this hypothesis by studying the origin and growth of these various unstable modes in concert with fluctuations in the strength and curvature of the easterly jet for realistic conditions.

## 6. Summary and Discussion

Global synoptic meteorological analyses of the MLT from the NOGAPS-ALPHA data assimilation system have provided, for the first time, a comprehensive description of variability in both Q2DW and migrating diurnal tide during the NH summers of 2007–2009. Unlike the SH case, where the Q2DW is primarily a westward propagating zonal wave number 3 feature, we find that the Q2DW in NH summer is composed primarily of

These calculations have also been performed for the summers of 2007 and 2008, and similar decreases in growth times from July to August were found in each case (not shown).

The results from these types of model calculations can be highly sensitive to the curvature of the zonal wind fields, and thus averaging or smoothing of the input dynamical fields can affect the results. We present these calculations to better understand, in a qualitative sense, possible factors that contribute to the observed intraseasonal variability of the NH Q2DW. From these results, we can conclude that the baroclinically unstable region along the equatorward flank of the NH summer easterly jet produces the fastest-growing modes at wave numbers 3–5. During June and July, the periods of the wave number 3 and 4 modes most closely match the 2 day period of the Rossby normal mode, and these grow preferentially over other modes.

These results alone do not explain why the observed [0.5,3] component of the Q2DW is larger during July while the [0.5,4] component is larger in June and August. Nor do they account for the sporadic behavior of the Q2DW which tends to produce the double peaked structure observed in, e.g., Figure 7. However,

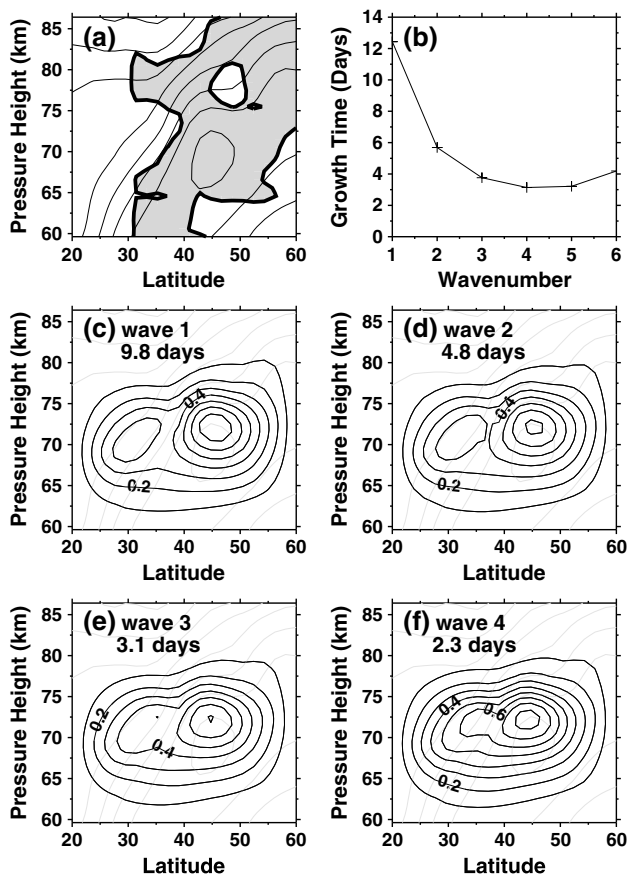


Figure 16. As in Figure 15 but for the 5 August 2009 case.

be controlled by the location of the critical line. The large wave number 3 amplitudes observed during July 2009 coincide with a relatively strong and well-defined easterly jet core that directed more wave activity upward compared to July 2007, when the jet core was smaller and weaker.

Results from a linearized instability model using daily NOGAPS-ALPHA winds for summer 2009 as input show that the baroclinically unstable region near the summer easterly jet supports growth of both zonal wave number 3 and 4 disturbances with periods near 2 days. The growth times of these disturbances are

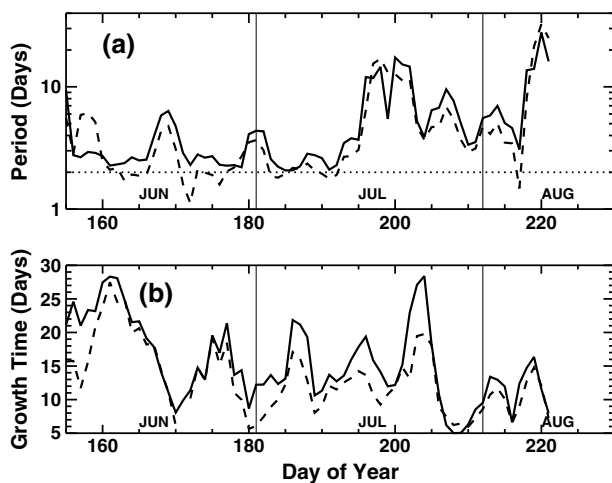


Figure 17. Time series of (a) period and (b) e-folding time for zonal wave number 3 (solid curve) and wave number 4 (dashed curve) instability model solutions during summer 2009. Dashed line drawn at 2 days.

typically in the range of 10–20 days during July, but approach ~5 days in early August. Using a similar modeling approach based on winds from a mechanistic global circulation model (GCM), *Rojas and Norton [2007]* found evidence for two zonal wave number 3 modes with growth times between 3 and 5 days: a faster growing mode with period of 35 h and a slower growing mode with a period of 42 h. In this study, *Rojas and Norton [2007]* found that the faster growing mode quickly reached saturation at relatively small amplitude while the slower growing mode continued to grow to much larger amplitude and then began to interact with the background flow. We plan to pursue this

Diagnostic calculations based on NOGAPS-ALPHA output indicate that the Q2DW originates from baroclinically unstable regions on the equatorward flank of the summer easterly jet near the 0.1 hPa level (~65–70 km). The vertical propagation of the Q2DW activity appears to

subject further by conducting free-running model simulations using the NOGAPS-ALPHA meteorological fields as initial conditions to determine whether the [0.5,3] component interacts with the [0.5,4] components as it grows, or if the two components grow independently from one other.

We do not find evidence for Q2DW-tide interaction that can sometimes lead to rapid amplification of the Q2DW in SH summer [e.g., Norton and Thuburn, 1999; Palo *et al.*, 1999; McCormack *et al.*, 2010; Hecht *et al.*, 2010; Chang *et al.*, 2011; Yue *et al.*, 2012b]. This is likely due to the smaller amplitudes and more broad band nature of the Q2DW in NH summer compared to SH summer, which reduces the chances for the type of interaction described by Walterscheid and Vincent [1996]. A modeling study of the SH Q2DW in January by Chang *et al.* [2011] found that nonlinear advection of momentum by the Q2DW itself may introduce variations in the background flow and, by extension, in tidal amplitudes that can also account for anticorrelation between the Q2DW and migrating diurnal tide. Other factors controlling the year-to-year variations in the strength and location of the NH summer easterly jet such as gravity wave activity [Ern *et al.*, 2013] may also play a role in controlling the behavior of both the Q2DW and tides. To further investigate the nature of possible coupling between the Q2DW, gravity waves, and tides in NH summer, a targeted series of global circulation model (GCM) experiments capable of accurately simulating the evolution of the background zonal flow throughout the NH summer MLT is needed. Recently, Sassi *et al.* [2013] used a GCM driven by NOGAPS-ALPHA meteorological fields in the lower atmosphere to generate a Q2DW in the SH summer MLT internally through baroclinic instability processes, rather than through means of an imposed forcing [e.g., Chang *et al.*, 2011]. A future study will use a similar approach for the NH summer cases of 2007–2009 to more closely examine possible sources of the interseasonal and interannual variability in the NH summer Q2DW presented here.

#### Acknowledgments

We thank three anonymous reviewers for their constructive comments. We thank Michael Stevens at the Naval Research Laboratory for his assistance with comparisons between NOGAPS-ALPHA and meteor radar winds. This work was supported in part by the Office of Naval Research and by the NASA Heliophysics Guest Investigator Program under award NNH09AK64I.

#### References

- Andrews, D. G., J. R. Holton, and C. B. Leovy (1987), *Middle Atmosphere Dynamics*, 489 pp., Academic Press, Orlando, Fla.
- Chou, M.-D., and M. J. Suarez (2002), A solar radiation parameterization for atmospheric studies, NASA Tech. Mem. 10460, 15, *Technical Report Series on Global Modeling and Data Assimilation*, edited by M. J. Suarez, 52 pp.
- Chou, M.-D., M. J. Suarez, X. Z. Liang, and M.-H. Yan (2001), A thermal infrared radiation parameterization for atmospheric studies, NASA Tech. Mem. 104606, 19, *Technical Report Series on Global Modeling and Data Assimilation*, edited by M. J. Suarez, 65 pp.
- Chang, L. C., S. E. Palo, and H.-L. Liu (2011), Short-term variability in the migrating diurnal tide caused by interactions with the quasi 2 day wave, *J. Geophys. Res.*, *116*, D12112, doi:10.1029/2010JD014996.
- Coy, L., S. D. Eckermann, K. W. Hoppel, and F. Sassi (2011), Mesospheric precursors to the major stratospheric sudden warming of 2009: Validation and dynamical attribution using a ground-to-edge-of-space data assimilation system, *J. Adv. Model. Earth Syst.*, *3*, M10002, doi:10.1029/2011MS000067.
- Daley, R., and E. Barker (2001), NAVDAS: Formulation and diagnostics, *Mon. Weather Rev.*, *129*, 869–883.
- Eckermann, S. D., K. W. Hoppel, L. Coy, J. P. McCormack, D. E. Siskind, K. Nielsen, A. Kochenash, M. H. Stevens, and C. R. Englert (2009a), High-altitude data assimilation system experiments for the Northern Hemisphere summer mesosphere season of 2007, *J. Atmos. Sol. Terr. Phys.*, *531*–551, doi:10.1016/j.jastp.2008.09.036.
- Eckermann, S. D. (2009b), Hybrid  $\sigma - p$  coordinate choices for a global model, *Mon. Weather Rev.*, *137*, 224–245.
- Eckermann, S. D. (2011), Explicitly stochastic parameterization of nonorographic gravity-wave drag, *J. Atmos. Sci.*, *68*, 1749–1765.
- Ern, M., P. Preusse, S. Kälisch, M. Kaufmann, and M. Riese (2013), Role of gravity waves in the forcing of quasi two-day waves in the mesosphere: An observational study, *J. Geophys. Res. Atmos.*, *118*, 3467–3485, doi:10.1029/2012JD018208.
- Garcia, R. R., R. Lieberman, J. M. Russell, and M. G. Mlynczak (2005), Large-scale waves in the mesosphere and lower thermosphere observed by SABER, *J. Atmos. Sci.*, *62*, 4384–4399.
- Gu, S.-Y., T. Li, X. Dou, Q. Wu, M. G. Mlynczak, and J. M. Russell (2013), Observations of Quasi-Two-Day wave by TIMED/SABER and TIMED/TIDI, *J. Geophys. Res. Atmos.*, *118*, 1624–1639, doi:10.1002/jgrd.50191.
- Harris, T. J. (1994), A long-term study of the quasi-two-day wave in the middle atmosphere, *J. Atmos. Terr. Phys.*, *56*, 569–579.
- Hartmann, D. L. (1983), Barotropic instability of the polar night jet, *J. Atmos. Sci.*, *40*, 817–835.
- Hecht, J. H., R. L. Walterscheid, L. J. Gelin, R. A. Vincent, I. M. Reid, and J. M. Woithe (2010), Observations of the phase-locked 2 day wave over the Australian sector using medium-frequency radar and airglow data, *J. Geophys. Res.*, *115*, D16115, doi:10.1029/2009JD013772.
- Hayashi, Y. (1971), A generalized method of resolving disturbances into progressive and retrogressive waves by space Fourier and time cross-spectral analyses, *J. Meteorol. Soc. Jpn.*, *49*, 125–128.
- Hogan, T., and T. Rosmond (1991), The description of the Navy Operational Global Atmospheric Prediction System's spectral forecast model, *Mon. Weather Rev.*, *119*, 1186–1815.
- Hoppel, K. W., N. L. Baker, L. Coy, S. D. Eckermann, J. P. McCormack, G. E. Nedoluha, and D. E. Siskind (2008), Assimilation of stratospheric and mesospheric temperatures from MLS and SABER into a global NWP model, *Atmos. Chem. Phys.*, *8*, 6103–6116.
- Lieberman, R. S. (1999), Eliassen-Palm fluxes of the 2-day wave, *J. Atmos. Sci.*, *56*, 2846–2861.
- Lima, L. M., P. P. Batista, H. Takahashi, and B. R. Clemesha (2004), Quasi-two-day wave observed by meteor radar at 22.7°S, *J. Atmos. Terr. Phys.*, *66*, 529–537, doi:10.1016/j.jastp.2004.01.007.
- Limpasuvan, V., C. B. Leovy, and Y. J. Orsolini (2000), Observed temperature two-day wave and its relatives near the stratopause, *J. Atmos. Sci.*, *57*, 1689–1701.
- Limpasuvan, V., and D. L. Wu (2003), Two-day wave observations of UARS Microwave Limb Sounder mesospheric water vapor and temperature, *J. Geophys. Res.*, *108*(D10), 4307, doi:10.1029/2002JD002903.
- Limpasuvan, V., and D. L. Wu (2009), Anomalous two-day wave behavior during the 2006 austral summer, *Geophys. Res. Lett.*, *36*, L04807, doi:10.1029/2008GL036387.

- Manney, G. L., and W. J. Randel (1993), Instability at the winter stratopause: A mechanism for the 4-day wave, *J. Atmos. Sci.*, *50*, 3928–3938.
- McCormack, J. P., S. D. Eckermann, D. E. Siskind, and T. J. McGee (2006), CHEM2D-OPP: A new linearized gas-phase ozone photochemistry parameterization for high-altitude NWP and climate models, *Atmos. Chem. Phys.*, *6*, 4943–4972.
- McCormack, J. P., L. Coy, and K. W. Hoppel (2009), Evolution of the quasi-two day wave during January 2006, *J. Geophys. Res.*, *114*, D20115, doi:10.1029/2009JD012239.
- McCormack, J. P., S. D. Eckermann, K. W. Hoppel, and R. A. Vincent (2010), Amplification of the quasi-two day wave through nonlinear interaction with the migrating diurnal tide, *Geophys. Res. Lett.*, *37*, L16810, doi:10.1029/2010GL043906.
- Muller, H. G., and L. Nelson (1978), A traveling quasi 2-day wave in the meteor region, *J. Atmos. Terr. Phys.*, *40*, 761–766.
- Norton, W. A., and J. Thuburn (1999), Sensitivity of mesospheric mean flow, planetary waves, and tides to strength of gravity wave drag, *J. Geophys. Res.*, *104*(D24), 30,897–30,911.
- Offermann, D., P. Hoffmann, P. Knieling, R. Koppmann, J. Oberheide, D. M. Rigglin, V. M. Tunbridge, and W. Steinbrecht (2011), Quasi 2 day waves in the summer mesosphere: Triple structure of amplitudes and long-term development, *J. Geophys. Res.*, *116*, D00P02, doi:10.1029/2010JD015051.
- Orsolini, Y. J., V. Limpasuvan, and C. B. Leovy (1997), The tropical stratopause response in the UKMO stratospheric analyses: Evidence for a 2-day wave and inertial circulations, *Q. J. R. Meteorol. Soc.*, *123*, 1707–1724.
- Palmer, T. N., G. J. Shutts, and R. Swinbank (1986), Alleviation of a systematic westerly bias in general-circulation and numerical weather prediction models through an orographic gravity-wave drag parametrization, *Q. J. R. Meteorol. Soc.*, *112*, 1001–1039.
- Palo, S. E., R. G. Roble, and M. E. Hagan (1999), Middle atmosphere effects of the quasi-two-day wave determined from a general circulation model, *Earth Planets Space*, *51*, 629–647.
- Pancheva, D. V. (2006), Quasi-2-day wave and tidal variability observed over Ascension Island during January/February 2003, *J. Atmos. Terr. Phys.*, *68*, 390–407, doi:10.1016/j.jastp.2005.02.028.
- Pendlebury, D. (2012), A simulation of the quasi-two day wave and its effect on variability of summertime mesopause temperatures, *J. Atmos. Sol. Terr. Phys.*, *80*, 138–151, doi:10.1016/j.jastp.2012.01.006.
- Pfister, L. (1985), Baroclinic instability of easterly jets with applications to the summer mesosphere, *J. Atmos. Sci.*, *42*, 313–330.
- Plumb, R. A. (1983), Baroclinic instability of the summer mesosphere: A mechanism for the quasi-two-day wave?, *J. Atmos. Sci.*, *40*, 262–270.
- Randel, W. J. (1994), Observations of the 2-day wave in NMC stratospheric analyses, *J. Atmos. Sci.*, *51*, 306–313.
- Rojas, M., and W. Norton (2007), Amplification of the 2-day wave from mutual interaction of the global Rossby-gravity and local modes in the summer mesosphere, *J. Geophys. Res.*, *112*, D12114, doi:10.1029/2006JD008084.
- Salby, M. L. (1981), The 2-day wave in the middle atmosphere: Observations and theory, *J. Geophys. Res.*, *86*(C10), 9654–9660.
- Salby, M., and P. Callaghan (2000), Seasonal amplification of the 2-day wave: Relationship between normal mode and instability, *J. Atmos. Sci.*, *58*, 1858–1869.
- Salby, M. L., and P. F. Callaghan (2008), Interaction of the 2-day wave with solar tides, *J. Geophys. Res.*, *113*, D14121, doi:10.1029/2006JD007892.
- Sassi, F., H.-L. Liu, J. Ma, and R. R. Garcia (2013), The lower thermosphere during the Northern Hemisphere winter of 2009: A modeling study using high-altitude data assimilation products in WACCM-X, *J. Geophys. Res. Atmos.*, *118*, 8954–8968, doi:10.1002/jgrd.50632.
- Singer, W., J. Bremer, W. K. Hocking, J. Weiss, R. Latteck, and M. Zecha (2003), Temperature and wind tides around the summer mesopause at middle and Arctic latitudes, *Adv. Space Res.*, *31*(9), 2055–2060.
- Stevens, M. H., et al. (2010), Tidally induced variations of PMC altitudes and ice water content using a data assimilation system, *J. Geophys. Res.*, *115*, D18209, doi:10.1029/2009JD013225.
- Suresh Babu, V., K. Kishore Kumar, S. R. John, K. V. Subrahmanyam, and G. Ramkumar (2011), Meteor radar observations of short-term variability of quasi 2 day waves and their interaction with tides and planetary waves in the mesosphere-lower thermosphere region over Thumba (8.5°N, 77°E), *J. Geophys. Res.*, *116*, D16121, doi:10.1029/2010JD015390.
- Teitelbaum, H., and F. Vial (1991), On tidal variability induced by nonlinear interaction with planetary waves, *J. Geophys. Res.*, *96*(A8), 14,169–14,178, doi:10.1029/91JA01019.
- Tunbridge, V. M., D. J. Sandford, and N. J. Mitchell (2011), Zonal wave numbers of the summertime 2 day planetary wave observed in the mesosphere by EOS Aura Microwave Limb Sounder, *J. Geophys. Res.*, *116*, D11103, doi:10.1029/2010JD014567.
- Walterscheid, R. L., and R. A. Vincent (1996), Tidal generation of the phase-locked 2-day wave in the Southern Hemisphere summer by wave-wave interactions, *J. Geophys. Res.*, *101*(D21), 26,567–26,576, doi:10.1029/96JD02248.
- Wu, D. L., P. B. Hays, R. W. Skinner, A. R. Marshall, M. D. Burrage, R. S. Lieberman, and D. A. Orland (1993), Observations of the quasi 2-day wave from the High Resolution Doppler Imager on UARS, *Geophys. Res. Lett.*, *20*(24), 2853–2856.
- Wu, D. L., E. F. Fishbein, W. G. Read, and J. W. Waters (1996), Excitation and evolution of the quasi-2-day wave observed in UARS/MLS temperature measurements, *J. Atmos. Sci.*, *53*(5), 728–738.
- Wu, Q., D. A. Orland, T. L. Killeen, R. G. Roble, M. E. Hagan, H.-L. Liu, S. C. Solomon, J. Xu, W. R. Skinner, and R. J. Nijciewski (2008), Global distribution and interannual variations of mesospheric and lower thermospheric neutral wind diurnal tide: 1. Migrating tide, *J. Geophys. Res.*, *113*, A05308, doi:10.1029/2007JA012542.
- Yue, J., W. Wang, A. D. Richmond, and H.-L. Liu (2012a), Quasi-two-day wave coupling of the mesosphere and lower thermosphere-ionosphere in the TIME-GCM: Two-day oscillations in the ionosphere, *J. Geophys. Res.*, *117*, A07305, doi:10.1029/2012JA017815.
- Yue, J., H.-L. Liu, and L. C. Chang (2012b), Numerical investigation of the quasi 2 day wave in the mesosphere and lower thermosphere, *J. Geophys. Res.*, *117*, D05111, doi:10.1029/2011JD016574.